Chapter 2. Extrinsic (Fast) Luminescence of Inorganic Fluorides

There are quite many papers as well as monographs dealing with extrinsic luminescence. This Chapter contains most general information about extrinsic luminescence and its applications for fast, dense scintillators based on heavy metal fluorides. For this reason, as well as in order not to make the book too long, some major and disputable problems pertaining to fast luminescence will not be reported in full.

The main goal of this Chapter is to update knowledge about the origin, mechanisms and parameters of fast luminescence due to impurities for a reader who may not be a specialist in physics of luminofors. This minimum data on fast extrinsic luminescence can be later used for choosing the approach for preparation of new fast scintillators for high energy physics.

2.1. Basic Principles of Extrinsic Luminescence

Extrinsic crystals are obtained by doping a pure host crystal with a small amount of impurities (metal ions) as activators for luminescence. The luminescence occurs in radioative recombination of self-trapped excitons of the activator. There are both the ground state and the first excited state of the activator in the forbidden energy gap, as illustrated in Fig. 2.1. The excitation

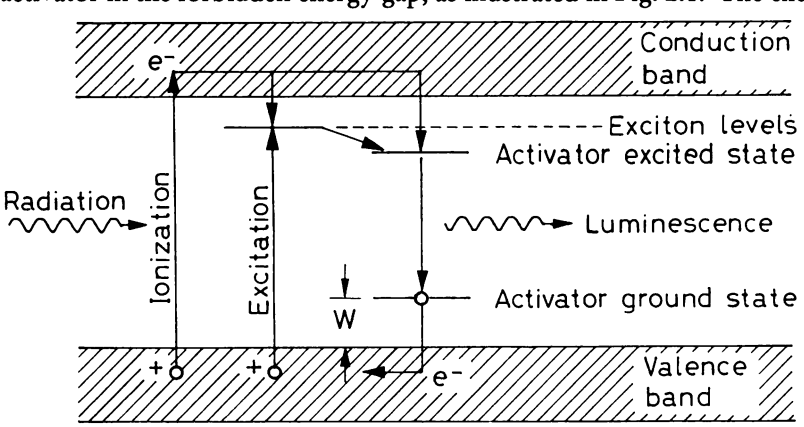

Fig. 2.1. Scheme of luminescence in extrinsic inorganic crystals.

occurs directly through absorption of the incoming radiation by the activator, or indirectly through energy transfer from the sensitizers [2.1], which are the network or impurity ions absorbing the excitation energy. The result is usually an excited activator atom, in which the electron in the excited state falls to the ground state, emitting a photon. Since the transition energy is smaller than the forbidden energy gap, the crystal is transparent to its own emission, which is usually in the visible range. Although many heavy extrinsic scintillators with efficient impurity induced luminescence are known among alkali halides (NaI:Tl, CsI:Tl, etc.), oxides (GSO:Ce, etc.) and so on, there are not many of them among fluorides. Typical examples of heavy extrinsic fluoride scintillators include LaF_3:Nd, BaF_2:Ce, etc.

The emission spectrum and the decay time characteristics of luminescence depend on the electronic transitions involved in the emission process. The specific site where the electronic transition occurs is called the luminescence (or emission) centre. Table II.1 gives a summary of well-known phosphors used for activators, classified according to the type of the electronic transition at the luminescence centre. The luminescence centre in many phosphors is one of rare-earth metals such as Eu, Nd, Ce, etc. The Table gives the luminescence decay times which are predictable to an order of magnitude, once the phosphor as well as the type of the electronic transition is specified. As seen in the Table, the decay time is in a wide span of 5 digits depending on the type of transition. In order to obtain fast luminescence as fast as tens of nanoseconds or faster, as is widely required for nuclear and high energy physics applications, $f \leftrightarrow d$ transitions are most important. The $5d \rightarrow 4f$ transition in rare earth ions is frequently utilized. Although the $4f^n$ electrons are shielded from the host crystal field by outer $5s^2$ and $5p^6$ closed shells, the $5d$ electron is less shielded, allowing the influence of the crystal field on the energy level. Consequently, the wavelength of the emission peak depends on the host crystals. Among such rare earth metallic ions, Ce^{3+} is known [2.2, 3] to give the fastest transition time constant as short as a few tens of nanoseconds.

Table II.1.
CLASSIFICATION OF ELECTRONIC TRANSITIONS IN SCINTILLATION CRYSTALS

Electronic transition	Luminescence centre	Typical phosphor	Decay constant(s)
$f \rightarrow f$	Pr^{3+}, Eu^{3+}, Tb^{3+}, Tm^{3+}	CaF_2:Eu	$10^{-4} \sim 10^{-3}$
$f \rightarrow d$	Ce^{3+}, Eu^{2+}, Nd^{3+}	Gd_2SiO_5:Ce, CeF_3, LaF_3	$10^{-8} \sim 10^{-7}$
$s^2 \rightarrow sp$	In^{1+}, Tl^{1+}, Bi^{3+}, Pb^{2+}	NaI:Tl, $Bi_4Ge_3O_{12}$	$\sim 10^{-8}$
complex ions	WO_4^{2-}, UO_2^{2+}	$CdWO_4$, $CaWO_4$	$\sim 10^{-5}$

Lately, a new form of extrinsic luminescence involving the hole transitions between the core impurity level and valence band has been investigated in some crystals. Extrinsic core-valence luminescence resembles, in a sense, intrinsic one. This is because the luminescence does not occur only in the activator, but as a result of interplay between both the activator cations and the fluorine anions in the host lattice. When an extrinsic scintillator is denoted as MF_m:R, with R as an activator, the overall luminescence is, in many cases, an overlap of two intrinsic luminescences, i.e., the excitonic and core-valence luminescence, if any, of MF_m, and the core-valence luminescence of RF_n. Since the efficiency of core-valence luminescence is not large (as small as 1 % level [2.4], or a few thousands photons per MeV deposited energy [2.5]), it is usually necessary to introduce large molar percentage of the activator into the host crystal, in order to obtain large light output. In this case, the doped MF_m:R crystal becomes similar to multicomponent crystals of $M_{1-x}R_xF_{(1-x)m+xn}$ with the close order of MF_m and RF_n contents.

There can be various aims of using a doped MF_m:R crystal instead of either MF_m or RF_n single component crystals, namely, to impart the crystal scintillating ability (when the host does not yield luminescence) or to obtain fast luminescence (when the host gives only slow exciton luminescence) and so on. When the host crystal yields core-valence luminescence, however, the doping can be made with other aims. It can improve light output, emission spectrum, material density, crystal quality (hygroscopicity, cleavage, transparency, etc.), radiation hardness, etc. In this case, various elements can be chosen for R, since R need not to be an origin of core-valence luminescence any more. Many studies on this problem have been performed, see, for example, the review in Chapter 4.

While the effect of doping of the host crystal is described above, the core-valence luminescence of RF_n itself can be modified, on the other hand, in the host crystal. When the atom M is much heavier than R, the threshold, E_{cc}, of the upper core band of the R ion with respect to the conduction band is expected to be increased. This tendency is seen in a comparison between ternary and binary fluorides. As an example, E_{cc} is increased by about 1 eV in RbY_2F_7 (or $KMgF_3$) compared with RbF (KF) [2.6]. In general, the *2p* valence band of fluorine and the upper core band of the activator, if it is an alkali or alkaline earth ion, can be affected by the host crystal field, since the electrons in both the above bands are not shielded by outer closed shells.

When the amount of dopant R is a small fraction of the host fluoride, which dopants are promising? Rb, Cs and Ba are promising candidates among alkali and alkaline earth metal ions from Li to Ba, since, as described in Chapter 1, RbF, CsF and BaF_2 give substantial core-valence luminescence at room temperature, for details, see Chapter 1. Extrinsic core-valence

luminescence has clearly been observed in KF:Rb [2.7]. It was marginal in KYF_4:Rb [2.5]. In BaF_2:Rb [2.5] no core-valence luminescence due to RbF was observed, but a reduction of the slow component (exciton luminescence) from BaF_2.

2.2. Characteristics of Fast Luminescence

As mentioned above, scintillators with nanosecond luminescence decay times are required for high energy physics at the modern level of developing detection systems. Let us consider some general and particular aspects of behaviour of scintillators with such parameters of luminescence.

2.2.1. Quenching of Luminescence. The luminescence may be quenched due to various causes. Typical quenching effects are (1) thermal, (2) impurity and (3) concentration quenching [2.8]. Among the above three quenching effects, the thermal one is the most popular and it exists in all intrinsic/extrinsic crystal scintillators with excitonic luminescence.

Thermal quenching can be most simply understood for extrinsic scintillators in which each luminescence center is isolated from the neighboring one. The surrounding crystal field is oscillating. In the simple harmonic oscillator model, each of the ground and the excited states of the luminescence centres can be expressed by a parabola in the configurational coordinate diagram [2.9, 10] as sketched in Fig. 2.2. Referring to this Figure,

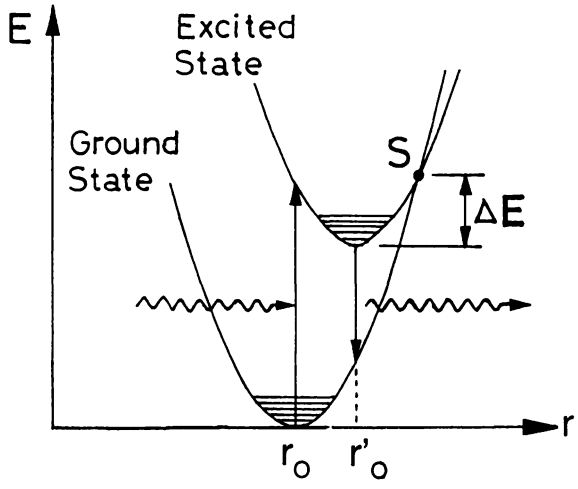

Fig. 2.2. The configurational coordinate diagram for activator ions

the excited electrons get the energy ΔE thermally to reach the crossing point S of the two parabolas. A transition from the excited to the ground state can take place here without emission of radiation but just with heat dissipation. The probability P_{nr} of this non-radiative transition is proportional to a Boltzman's factor exp(-ΔE/kT) where k is the Boltzman constant, while the radiative transition probability P_r is not affected by temperature. Consequently, the luminescence efficiency becomes:

$$\eta = P_r/(P_r + P_{nr}) = [1 + C_t \exp(-\Delta E/kT)]^{-1}$$

with C_t as a constant. Thermal quenching causes reduction both in intensity and in decay time of luminescence as the temperature increases. In a typical fluorite scintillator CeF_3 thermal quenching occurs around 370 K [2.11] as seen in Fig. 2.3.

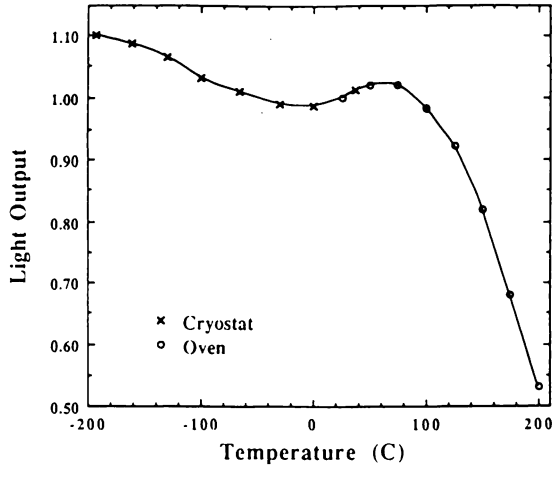

Fig. 2.3. Thermal quenching in CeF_3 [2.11].

The energy E is plotted versus configurational coordinate *r* which is the distance between the dopant ion and the surrounding ions. r_o (r_o') denotes the ground (excited) state with the lowest energy.

When the luminescence is slow, there exists enough time during which thermal quenching should compete with radiative transition. Moreover, the excitation energy of the luminescence centres is sometimes transferred indirectly from the sensitizers which absorb the excitation energy. In the course of energy transfer the probability of non-radiative transition to the

valence band should increase with temperature. *Consequently, the thermal quenching is expected to be qualitatively larger for slow luminescence than for the fast one.*

When the two parabolas of the ground and the excited states sketched in Fig. 2.2 are not much separated in the configurational coordinate (i.e., weak coupling), the probability of their crossing each other is small, as far as one phonon transition is concerned. In this case, the Stokes shift must be small. Consequently, the tendency of small temperature quenching is expected in crystals of small Stokes shifts.

In some scintillators, for example, CsI:Tl [2.12, 13], light output once increases with temperature, reaches a maximum and starts to quench. Referring to the band structure shown in Fig. 2.1, the increase in luminescence intensity can be understood as follows: when the temperature is increased, more and more electrons in the trapping levels, slightly below the conduction band, can be raised to the conduction band. Then, some of the electrons can reach the luminescence centre (the excited state of the activator), resulting in luminescence.

The impurity quenching is thought to occur through the action of 'killer' centers [2.8]. Introduction of certain impurities into the lattice, especially heavy metals such as Cu, Fe, Co, Ni, Cr, etc. may create the so-called 'killer' centres (trapped holes) lying between the valence and the conduction bands. Electrons in the valence band may be raised to the luminescence centres (activator ground state in Fig. 2.1), releasing the holes trapped in the activator ground state. These new holes in the valence band migrate and are trapped at other centres, called 'killer' centres, due to impurities. The electrons in the excited states of the luminescence centres can now recombine with the 'killer' centres non-radiatively due to phonon interaction, instead of dropping to the activator ground state by emitting luminescence. Consequently, the non-radiative transition probability P_{nr} which should be proportional to the population of the 'killer' centres, is proportional to exp(-W/kT) where W is the energy level of the luminescence centre measured from the valence band (see Fig. 2.1). The resultant luminescence efficiency becomes:

$$\eta = P_r/(P_r + P_{nr}) = [1 + \tilde{N}_i \exp(-W/kT)]^{-1}$$

where C_i is the constant which is proportional to the concentration of impurities.

The **concentration quenching** depends on the concentration of the activator dopant. It has been known for many scintillating crystals that, as the

dopant concentration increases, the luminescence increases first, reaches the maximum and starts to decrease again.

One of the possible mechanisms of the occurrence of the concentration quenching is as follows: in many scintillators, ionization energy is transferred from the host to the activator ions. The electrons in the conduction band and the holes in the valence band move to the activator to form excited states. Radiative recombination of the electron with the hole yields luminescence. When the dopant atoms are too abundant, some of the electrons at the excited levels cannot find out a hole in the same dopant atom, since the number of holes is limited by the number of ionization. Then, radiative recombination cannot occur, the electrons will drop non-radiatively to the ground state of the dopant or the host crystal within a long period.

The optimum dopant concentration usually varies between 0 and 1 % as seen in GSO:Ce [2.14, 15]. In both NaI:Tl and CsI:Tl, however, the concentration quenching is small: the light output rises sharply with the amount of Tl and almost levels off above 0.05 mole % up to 0.3 mole % for CsI:Tl [2.16, 17, 18] or 0.4 mole % for NaI:Tl [2.19], the maximum amounts of Tl are described in the above papers. For fluoride scintillators, the optimum amount of Ce in BaF_2:Ce is also between 0 and 1 % [2.20, 21, 22] as seen in Fig. 2.4. In this Figure, solid circles give the total light output, which is a sum of the three components, i.e. fast and slow components from BaF_2 and a 40 ns component from the $5d \rightarrow 4f$ transition in Ce^{3+}. Open circles give the percentage of the 40 ns component. The light output of Ce^{3+}

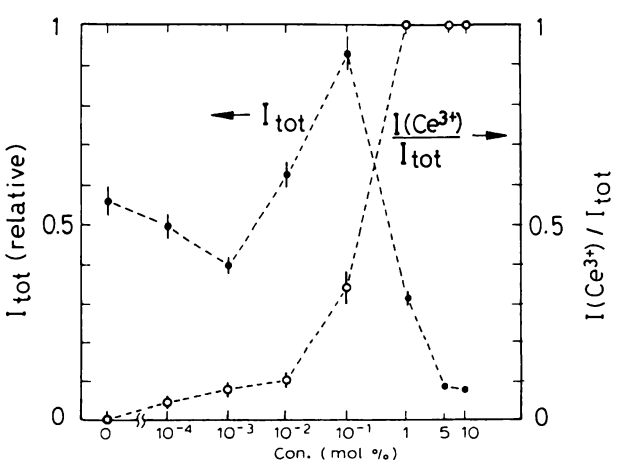

Fig. 2.4. Concentration quenching in BaF_2:Ce [2.22]. I_{tot} = total light output consisting of three components, 800 ps, 50 ns and 600 ns. I (Ce^{3+}) denotes the 50 ns component due to $5d \rightarrow 4f$ transition in Ce^{3+}.

is given by the product of the solid and open circles. For LaF_3:Nd, however, the 173 nm component due to the $5d \rightarrow 4f$ transition in Nd^{3+} does not yet start to quench at 3 mole % [2.23]. The interband luminescence due to $4f \rightarrow 4f$ transitions shows a maximum at a Nd concentration of 1 mole %. The observed quenching is understood in terms of cross relaxation in the same $4f$ band [2.23].

2.2.2. Quenching of Core-Valence Luminescence. Among the three quenching effects, which were described above for the usual luminescence, the first two (thermal and impurity quenching) are expected to occur also for core-valence luminescence, whereas the third one (concentration quenching) is not. While the thermal quenching is expected for most crystals with core-valence luminescence, many types of the core-valence luminescence including BaF_2 [2.24], CsF, RbF [2.6], $KMgF_3$, $KCaF_3$ [2.21, 25] do not exhibit thermal quenching at room temperature but far above it. For example, [2.24], the 220-nm component of BaF_2 due to core-valence luminescence is not quenched up to at least 358 K, while the 315-nm one due to excitonic luminescence monotonously decreases with the temperature increase from 198 to 358 K (see Fig. 2.5] Exceptions are, for example, KF [2.7], CsI [2.26]

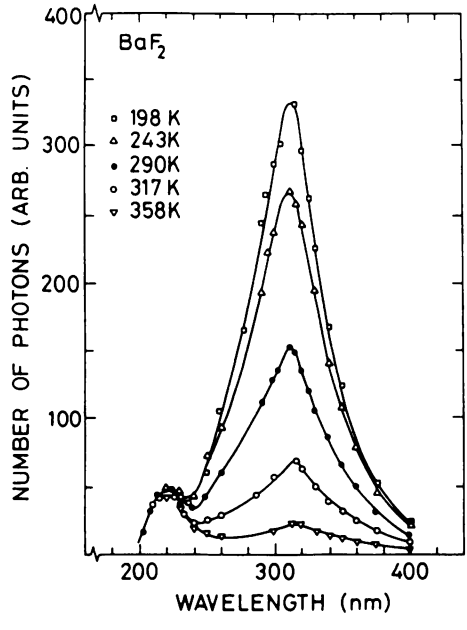

Fig. 2.5. Temperature dependences of core-valence and excitonic luminescence in BaF_2 [2.24].

and CsBr [2.27]. They show quenching by more than an order of magnitude between 80 and 300 K. In these crystals, the core-valence luminescence energy E_{cc} partially overlaps with the energy gap E_g between the valence and conduction bands, allowing the Auger electron emission. When the temperature increases, the overlap can be enhanced due to an increase in band widths, resulting in thermal quenching. Impurity quenching is also expected to occur for core-valence luminescence, but according to a different mechanism. Recombination of the excited electrons of activators with the 'killer' centres will not play any important role in quenching of the core-valence luminescence. On the other hand, when the excited levels of impurities exist below the conduction band with the excitation energy smaller than the core-valence luminescence, absorption of the core-valence luminescence by the impurities, similar to the Auger process, is allowed. An example is seen in BaF_2:La [2.28], when the amount of La, taken here as an impurity rather than as an activator, is increased, the 195 and 220 nm components of the core-valence luminescence are quenched much less than the 310 nm each due to excitonic luminescence.

For concentration quenching in core-valence luminescence, the situation is as follows. When the amount of dopant is increased, the core-valence luminescence related to the dopant is expected to increase, although there are few publications on the subject. For example, in KF:Rb [2.7] the core-valence luminescence becomes the same as in RbF when the amount of Rb is increased to a maximum.

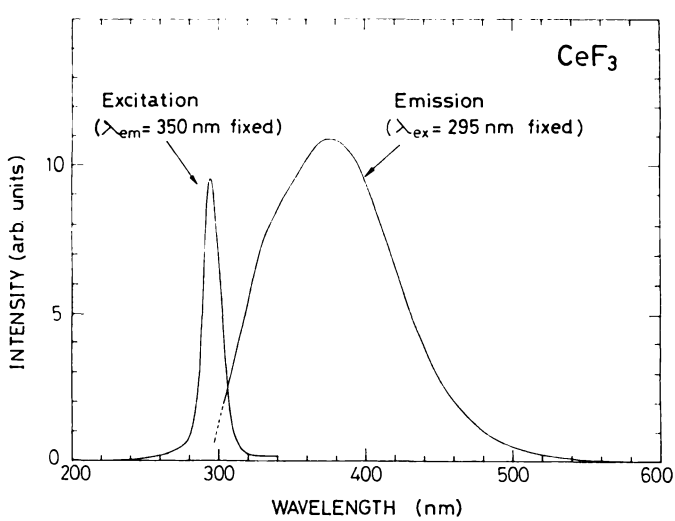

Fig. 2.6. Excitation and emission spectra of CeF_3 [2.29].

2.2.3. Light Output. Fig. 2.6 shows UV excitation and emission spectra of CeF_3, a typical fluoride scintillator. Since the emitted light is usually detected with photomultiplier tubes (PM-tubes) or photodiodes (SiPDs), a good spectrum matching between the emission and sensitivity of the detectors is important. The matching in wavelengths of 400 - 500 nm should be good with PM-tubes having a bialkali photocatode, while in 500 - 600 nm with SiPDs.

For the core-valence luminescence, the emission is usually in the UV range below 300 nm or even in the VUV range. It is 220 nm in BaF_2, one of the most familiar fluorides with core-valence luminescence. Measurement of UV light with photomultipliers or photodiodes is not so simple as that of visible light. Typical measuring methods are as follows:

a) use of **photomultipliers with a UV-sensitive photocatode** (such as Cs-I, Cs-Te, multialkali, etc.) and a quartz window. Sometimes, optical filters are used at the same time in order to remove longer wavelengths components, which are sometimes slower than the UV component. For example, luminescence in BaF_2 consists of two components, a fast one (0.6 ns) peaked at 220 nm and a slow one (600 ns) at 310 nm with the intensity ratio of about 1 to 3 (see a sketch in Fig. 2.7). There are many techniques of selective detection of only the fast component: use of quartz window PM-

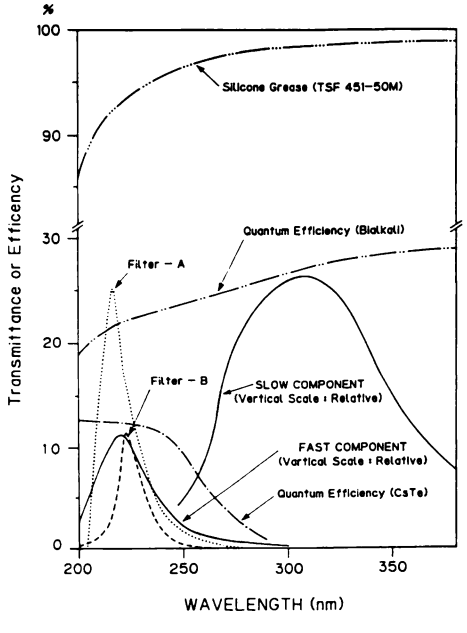

Fig. 2.7. Comparison of emission spectra of BaF_2 with the spectral sensitivities of photocatodes of photomultipliers and transmitance of typical filters etc. from [2.33].

tubes [2.30], solar blind Cs-Te PM-tubes [2.31, 32, 33], band-pass filters [2.33], wavelength filters [2.34], etc.;

b) **conversion of UV to visible light** by wavelength shifter materials, which are sometimes added to plastic scintillators, and subsequent detection with ordinary photomultipliers or photodiodes. Use of wavelength shifters between BaF_2 and photon detectors has been studied in order to use photomultipliers [2.35] or photodiodes [2.36], without any attempts to select only fast components;

c) **conversion of UV light to ionized electrons** in gas containing UV-photon sensitive ionizing material, i.e., with a low ionization potential, such as TMAE, TEA, etc. and subsequent registration of the electrons with discharge chambers [2.37, 38, 39, 40].

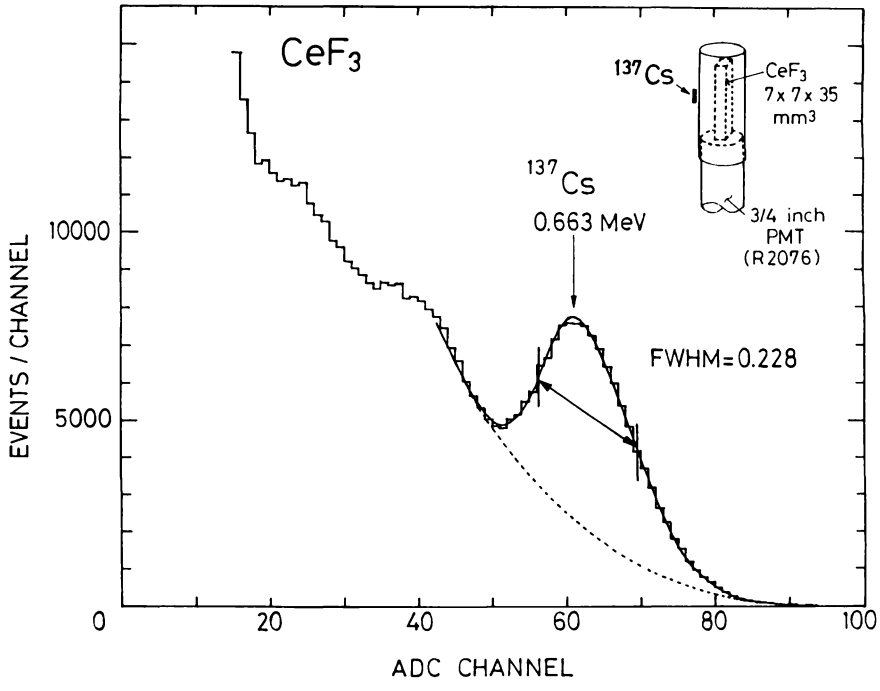

Fig. 2.8. Pulse height spectrum of ^{137}Cs γ-rays in CeF_3 [2.29].

Fig. 2.8 shows an energy spectrum of γ-rays from ^{137}Cs measured with a CeF_3 scintillator mounted on a photomultiplier. Light output can be compared for different scintillators of similar sizes from the positions of the γ-ray peak at 0.662 MeV. More or less absolute estimation is possible from the

energy resolution of the γ-ray peak on the assumption that the energy resolution is determined by photoelectron statistics. This assumption should hold for small transparent crystals with a full coupling with a photocatode with a good optical contact. Another method to estimate the absolute light output is measurement of pulse height for γ-rays with a known energy, for example, 0.662 MeV γ-rays from ^{137}Cs with a photomultiplier whose pulse height is already calibrated for a single photoelectron. It should be noted that the light output, estimated by the above methods, depends on the spectral sensitivity of the photomultipliers or photodiodes. Although correction for spectral sensitivity is necessary to obtain rigorously absolute light output independent of the photon detectors, it is usual to refer to the light output without the above correction, since the uncorrected values are practically more useful for detection of the light with the relevant photon detectors. An efficient scintillator corresponds to a large light output and small energy resolution. These parameters are closely related to the scintillation efficiency itself as well as to defects, optical quality, uniformity, etc. The above considered methods for detection of light output yield reliable results at the level of 0.1 per cent of NaI:Tl. The technique of determination of a lower light output is described in Chapter 6.

2.2.4. Decay Constants. The time evolution of the intensity of emission I_o after the end of excitation, t = 0, is approximately given by

$$I(t) = I_o \exp(-t/\tau)$$

in the simplest case of a single emission centre. Here I_o denotes the light output at t = 0 and τ is the decay time of luminescence.

In some scintillators, however, the rise time of luminescence is finite as is typically seen for GSO:Ce in [2.41]. The finite rise time should be due to slow build-up of luminescence centres after ionization. Consequently, the above case may occur only in excitonic or impurity induced luminescence and not in core-valence luminescence. In the approximation of an exponential population of the excited level, the time evolution becomes:

$$I(t) = I_o[\exp(-t/\tau) - \exp(t/\tau_p)],$$

where τ_p denotes the time constant that describes the energy transfer to the excited level. Basically, both the time constants of τ and τ_p depend on the mechanism of electronic transition at the luminescence centre.

Sometimes there are more than one luminescence centres. For example, in an orthosilicate crystal of GSO:Ce (or LSO:Ce), the Gd^{3+} (Lu^{3+}) ions occupy two distinct sites, one is surrounded by 7 (6) oxygen ligands and

the other by 9 (7) oxygen ligands. Since the Ce^{3+} ions occupy the same sites as the Gd^{3+} (Lu^{3+}), there are two different crystal fields filled by the Ce^{3+}, leading to two components [2.42]. In the case of *n*-emission centres, both the first and the second terms in the above equation should be, in principle, replaced by a sum of n-terms. When one sees the shapes of luminescence pulses in actual scintillators, however, the rise time is not large and it can be approximated by one effective value. So, it should be practical to fit the experimental time evolution curve by:

$$I(t) = \Sigma_{i=1}^{n} I_i \exp(-t/\tau_i) - I_o \exp(-t/\tau_p),$$

with $I_o = \Sigma_{i=1}^{n} I_i$. The decay time constant should be as short as possible when the counting rate in detectors is high.

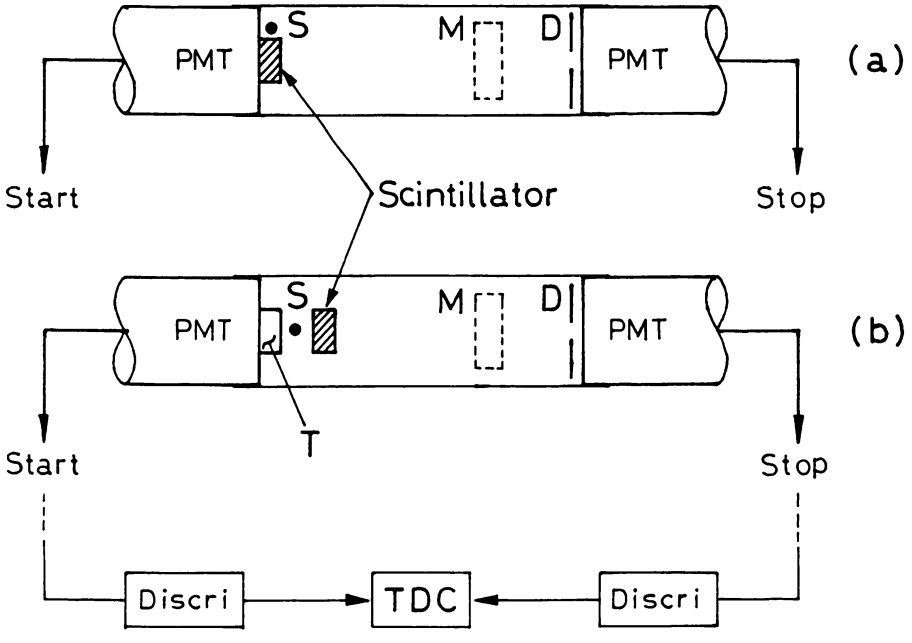

Fig. 2.9. Schematic setup to measure time evolution of luminescence in the single photoelectron techniques:

a) single scintillator;

b) separate scintillators schemes. D - diaphragm, S - radioactive source for isotopes, such as ^{60}Co, etc. T - fast efficient scintillator for generating a start signal in the case (b), and M - monochromator if necessary.

Measurement of decay time constant as well as the build-up time constant τ_p can be measured by various methods. When the time constants are much slower than 5 ns, they can be simply measured by analyzing the pulse shapes recorded with commercially available wave digitizers, whose speed is as high as 500 MHz. When the time constants are as fast as or faster than the above value as in many fluoride scintillators, single photoelectron techniques [2.43 - 45] have been used with a sufficiently good resolution. There are two possible schemes, a single-scintillator one and a separate-scintillators one, as sketched in Fig. 2.9. In both schemes, the start pulse is taken with a large light output in order to get a precise start timing, while the stop pulse is taken from the investigated scintillator after reduction of the light intensity entering the photomultiplier to one photoelectron levels. When the total light output from the investigated scintillator is large, both schemes can give an exact time of the start. But when the light intensity is small, only the separate scintillators scheme can give a good resolution in start timing. If necessary, a monochromator can be placed between the investigated scintillator and the photomultiplier for stop signals in order to study the decay time spectra of specific wavelength components.

2.3. General Characteristics of Crystals for Scintillators

2.3.1. Absorption of Incident Quanta and Particles. The large absorption coefficient is usually important, for example, in X-ray or positron-emission tomographers (PET) not only in order to make the detector size compact but also to improve space resolution. Good space resolution is sometimes especially important in detectors for nuclear as well as high energy physics experiments. When the incoming radiation has an intensity I_o, the intensity, having passed through a material thickness d, is approximately given by:

$$I = I_o \exp(-\mu d),$$

where μ is the linear absorption coefficient of the material. Sometimes, μ/ρ $(g/cm^2)^{-1}$ is used instead of μ (in cm^{-1}), since the former does not depend on the phase (solid or liquid or gas) of the material. The μ is related to the absorption cross section σ through a relation of:

$$\mu/\rho = \sigma N_a/A,$$

with N_a = Avogadro number ($N_a = 6.022 \times 10^{23}$) and A = the atomic mass.

The linear absorption coefficient can be divided in three according to different mechanisms of absorption as: $\mu = \mu_1 + \mu_2 + \mu_3$. Here μ_i denotes the

absorption due to photoelectric effect, Compton diffusion and electron pair creation and photonuclear reaction. At low energies (< 0.5 MeV) where the photoelectric effect is predominant, μ/ρ is roughly proportional to Z^4. In the intermediate energy range where the Compton effect is important, μ/ρ is independent of Z. At high energies (>> 1 MeV), μ/ρ is proportional to Z due to a dominance of electron pair creation. The magnitudes of μ_i's are given in [2.2] (above 1 MeV) and [2.46] (down to 1 KeV) for various elements.

The absorption coefficient for a compound denoted by a formula $A_xB_yC_z$ is given by:

$$\mu/\rho = w_a(\mu/\rho)_a + w_b(\mu/\rho)_b + w_c(\mu/\rho)_c,$$

where $(\mu/\rho)_a$ is the absorption coefficient divided by the density for A, and w_a is the weight ratio of A in the compound, given by:

$$w_a = xM_a/(xM_a + yM_b + zM_c),$$

where M_a, M_b and M_c are the atomic masses of A, B, C, respectively.

2.3.2. Effective Atomic Number, Radiation Length and Moliere Radius. There are some useful parameters which characterize, in a sense, compactness of the material, effective atomic number (Z_{eff}), radiation length (X_o), Moliere radius (R_M), etc.

At low energies, X-rays are absorbed predominantly by a photoelectron effect, for which the absorption coefficient is proportional to Z^4 in an approximation of linearity between the atomic mass and Z. It is convenient to use the effective atomic number Z_{eff} for a compound in the discussion of X-ray absorption ability. The Z_{eff} for the above-mentioned compound $A_xB_yC_z$ is given by the following equation:

$$Z_{eff} = (w_aZ_a^4 + w_bZ_b^4 + w_cZ_c^4)^{1/4}.$$

Here, Z_a, Z_b, Z_c are the atomic numbers of A, B and C, respectively.

When the energy of photons or electrons (positrons) is much higher than the critical energy ε_c, the energy loss is dominated by an electromagnetic shower of bremsstrahlung and pair production. ε_c is defined for electrons as the energy at which the energy loss due to ionization (the cross section being proportional to Z), is equal to that due to radiation (proportional to Z^2). ε_c is approximately inversely proportional to Z and is roughly given by 580 MeV (see [2.46] ε_c for various materials). In describing the longitudinal development of the shower in a material, it is convenient to measure the

longitudinal thickness in units of the radiation length X_o, which corresponds to the mean free path of an electron in the material and is determined by bremsstrahlung. The longitudinal development of the shower is approximately universal in units of X_o, regardless of the materials. X_o is approximately given in [2.47] by:

$$X_o^{-1} = C_o Z^2 \ln (183\, Z^{-1/3}),$$

where $C_o = 4\alpha\rho r_e^2 N_a/A$, $\alpha = 1/137$, and $r_e = e^2/mc^2 = 2.82.10^{-13}$ cm - the classical radius of electron. X_o for a compound, as mentioned in 2.3.1, is given by:

$$X_o^{-1} = C_o[xZ_a^2 \ln (183\, Z_a^{-1/3}) + yZ_b^2 \ln (183\, Z_b^{-1/3}) +$$

$$+ zZ_c^2 \ln (183\, Z_c^{-1/3})].$$

The mean free path (i.e. the absorption length) of a high energy photon is determined by pair production and is approximately equal to $9X_o/7$. When an electron or a photon with an energy E enters a material, multiplication of secondary particles (e^-/e^+, γ) occurs by repeating pair production and bremsstrahlung until the energy of each secondary particle becomes as low as ε_c. The shower maximum, which is defined by the maximum number of secondary particles, occurs at a longitudinal depth given by:

$$t_{max}(\text{in } X_o) \sim 1.01\, [\ln (E/\varepsilon_c)^{-\alpha}]$$

with $\alpha = 1$ for a primary electron beam and 0.5 for a primary photon beam, [2.47]. The lateral development does not necessarily scale in X_o. The lateral spread is dominated by the multiple scattering angle of electrons or positrons in the shower, given by:

$$[< \theta^2 >]^{1/2} \sim (21\ \text{MeV}/E)^*(t/X_o)^{1/2},$$

with t - the longitudinal thickness of material.

A universal unit for the lateral spread, the so-called Moliere radius R_M is defined as the rms lateral spread of electrons of energy ε_c after passing through one X_o:

$$R_M = (21\ \text{MeV}/\varepsilon_c)^* X_o.$$

R_M is larger (smaller) than X_o when ε_c is smaller (larger) than 21 MeV, i.e., when Z is larger (smaller) than ~ 29 (Cu). R_M for the above-mentioned compound $A_xB_yC_z$ can be calculated by substituting into the above formula the ε_c for the compound:

$$\varepsilon_c = [u_a\varepsilon_c(A) + u_b\varepsilon_c(B) + u_c\varepsilon_c(C)]/(u_a + u_b + u_c),$$

where the weight $u_a = w_a/(X_o\rho)_a$, and so on.

Electromagnetic showers are localized in a smaller longitudinal (lateral) space in the material with smaller X_o (R_M). For example, for 1 GeV γ -rays in heavy materials such as Pb or Pb-glass, about 95 % of the shower energy is contained within ~ 15 X_o longitudinally [2.48], and about 90 % within a radius of 1 R_M laterally [2.49].

2.3.3. Radiation Damage and Process of Recovery. Radiation detectors are sometimes used in strong radiation fields. The radiation sources may be various: protons, neutrons, mesons, electrons, γ-rays and other particles from particle accelerators, nuclear reactors, cosmic rays, etc. Since the radiation detectors that consist of single crystals usually owe their good performance to optical transparency and luminescence ability of the crystals, any damaging effects on these two properties are dangerous.

The primary effect of radiation damage is degradation in transparency rather than that in luminescence [2.50 - 53]. Degradation in transmittance is especially dangerous in γ-detectors for high energy physics, because even a small decrease in transmittance per X_o should accumulate over as long as 20 X_o and more.

Another effect is activation of the material. It becomes grave [2.50, 54, 55] when the crystals, especially those which contain heavy elements, are irradiated by hadrons (protons, neutrons, mesons, etc.). However, in most detectors in actual environments, unless they are directly hit by intense (primary or secondary) accelerator beams, the activation does not cause a big problem, because the activation decays much faster than builds up and its effect is usually limited to below 1 MeV. The role of activation will be considered in Chapter 6.

Consequently, degradation in optical transmission, in other words, solarization, should be the most important and the most extensively studied effect of radiation damage.

The mechanism may be different for the γ-ray (or electron) induced damage and the hadron induced one. Upon irradiation by γ-rays (or electrons), the crystal lattice should experience ionization or small recoil due to pair production, bremsstrahlung (electron or nucleon), Compton

scattering, etc. Since the recoil is usually small, the lattice ions could only slightly be displaced from the equilibrium positions. The displacement could be partly or mostly restored in time by thermal perturbation. Consequently, the only remaining effect should be related with trapped electrons to be discussed below.

When hadrons hit crystals, the situation can be different from the above. The interaction of hadrons with the ions in the crystal (or any nucleons in the ions) is much stronger than the electromagnetic interaction. The ions may be permanently displaced, or driven out from their original lattice positions, or fragmented into light atoms and/or nucleons, resulting in the static point defects in the lattice. Such a qualitative picture of hadron-induced damage can explain the smallness or saturation of its recovery with time or by thermal or UV (optical) annealing ([2.50] for BGO, [2.54] for GSO:Ce).

In a simple model, the radiation damage caused by γ-ray irradiation can be explained in the following way: when a crystal is irradiated, the valence electrons are excited to the exciton levels or ionized to the conduction band. Some of them can be trapped in trapping levels which lie between the valence and the conduction bands (see fig. 2.10 a, [2.56, 57]). Although the trapping centres may be metastable excited levels of the network atoms or the levels of impurities, the impurities seem to be most important in many cases, as seen in the results of various measurements of radiation damage [2.50, 22]. Besides the *F* center-like defects mentioned above, hole traps can occur upon movement of the hole from the valence band, as sketched in Fig. 2.10.

For BGO, a typical scintillator with excitonic luminescence, the band gap E_g is about 4 eV (from the low energy edge of the excitation peak) and the trapping centres lie roughly at E_t = 3.6 eV [2.58] above the valence band which is determined from measurements of the total light absorption over 400 to 600 nm as a function of irradiating UV wavelength. The trapped electrons, *F*-centre-like defects, give color to the crystal by absorbing light. They are raised to the conduction band and can finally return to the valence band non-radiatively. When $E = E_g - E_t$ is small (0.4 eV in BGO), the recovery occurs spontaneously at room temperature, since the thermal energy is sufficient to release the trapped electrons to the conduction band (see Fig. 2.10).

For BaF_2, a typical scintillator with core-valence luminescence, E_g is much larger, i.e., about 11 eV [2.59]. The trapping centres must sit, however, rather close to the conduction band as shown later in this paragraph, but not so close as in BGO, since spontaneous recovery is weak [2.52]. When spontaneous recovery is weak, recovery can be helped by heating (thermal annealing) or by exposure to UV light (UV annealing). For BaF_2, thermal as

well as optical annealing (or bleaching) was extensively studied [2.52, 53, 60]. The radiation damage in BaF_2 is almost fully recovered either by thermal annealing at 500 °C for three hours or by optical annealing with a 300 nm light source for a certain period as long as 10 hours. This result indicates that the trapping centres sit rather close (within a few eV) to the conduction band.

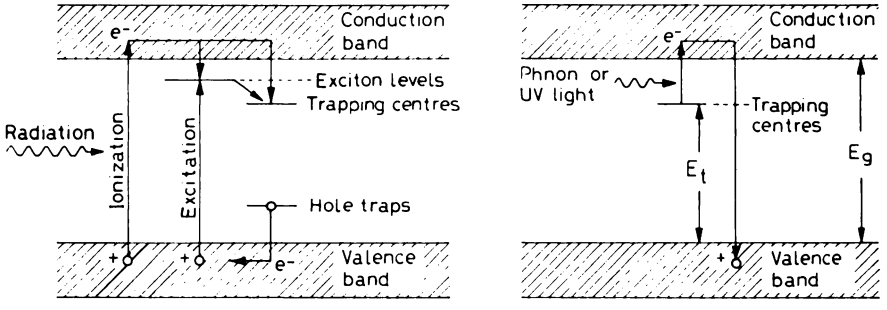

Fig.2. 10. (a) Electron trapping by γ-ray irradiation and (b) recovery of radiation damage.

When compared with thermal annealing, optical annealing seems to be a little complicated in some crystals. For example, BGO shows an almost full recovery by thermal annealing (400°C, 2 hours, [2.61]), but darkens upon UV exposure [2.50]. This darkening may be due to dominance of damage rather than annealing, since E_t is small (about 3.6 eV). When the light of lower energies (633 or 514 nm) is used so as not to cause radiation damage, recovery was observed to some extent [2.58]. Another example is GSO:Ce having cut-off wavelength of transmission at about 400 nm. In this crystal, UV annealing may not be expected to be very efficient as seen in the experiment [2.62]. On the other hand, thermal annealing may be difficult in practice for some crystals due to degradation of crystal surface caused by reaction at high temperatures. When BaF_2 is annealed at 500°C in air, a slight degradation of the crystal occurs. It is explained by surface pyrohydrolysis and can be removed by polishing [2.63]. CeF_3 slightly looses transparency [2.64] when it is annealed at 300°C in vacuum (10^{-3} Torr).

It should be noted, however, that removal of the surface layer of the crystal does not always cause recovery of the transparency, which is lost due to thermal treatment. In some fluorides and other materials the chemical and phase compositions are changed in the entire bulk. Transparency of such

crystals can be recovered by means of more complicated technological processes.

Definitions of radiation hardness are not the same in different publications. Usually this terminology has been used as a measure for the maximum dose tolerated in actual detectors. Such tolerable dose may depend on the depth of the detector. Since radiation hardness is usually important in detectors for high energy physics experiments, the necessary depth of the crystal is as large as 20 - 23 X_0.

It would be reasonable to define radiation hardness as a dose rate which should significantly reduce the transmittance at the emission peak wavelength, i.e., by 20 - 40 %, that corresponds to a 1 - 2 % reduction per X_0.

Even after this definition is adopted, radiation hardness still remains a parameter which is changed significantly from one crystal to another. It is often affected by uncontrolled factors. These points will be considered in more detail in Chapter 6. The above definition of radiation hardness will be corrected below when applied to the stage of search.

REFERENCES

2.1. Blasse G., Brill A., Characteristic Luminescence, Philips Tech. Rev., 1970, v. 31, No. 10, 303 - 332.

2.2. Moses W.W., Derenzo S.E., Cerium fluoride, a new fast, heavy scintillator, IEEE Trans. Nucl. Sci., 1989, v. 36, No. 1, 173 - 176.

2.3. Weber M.J., Cerium-activated crystal and glass scintillators, Intern. Workshop Crystal 2000, 22-26 September 1992, Chamonix, France, Proceedings, 99 - 124.

2.4. Rodnyi P.A., Core-valence transitions in wide-gap crystals, Sov. Phys. Solid State, 1992, v. 34, Np. 7, 1053 - 1066.

2.5. Dorenbos P., Visser R., van Eijk C.W.E., Valbis J., Khaidukov N.M., Photon yields and decay times of cross luminescence in ionic crystals, IEEE Trans Nucl. Sci., 1992, NS-39, No. 4, 506 - 510.

2.6. Aleksandrov Yu.M., Markov V.N., Khaidukov N.M., Yakimenko M.N., Excitation spectra of cross luminescence generated in alkali metal fluorides, Sov. Phys. Solid State, 1989, v. 31, 1609 - 1610.

2.7. Jansons J.L., Kurmins V.J., Rachko Z.A., Valbis J.A., Luminescence due to radiative transitions between valence band and upper core band in ionic crystals (Crossluminescence), Solid State Comm., 1988, v. 67, 183.

2.8. McKeever S.W.S., Thermoluminescence of Solids, Cambridge Univ. Press, Cambridge, 1985.

2.9. Blasse G., Luminescence of inorganic solids: from isolated centres to concentrated systems, Prog. Solid. State Chem., 1988, v. 18, 79 - 170.

2.10. Blasse G., Interaction between optical centres and their surroundings : an inorganic chemist's approach, Adv. Inorg. Chem., 1990, v. 35, 319 -402.
2.11. Anderson D.F., Cerium Fluoride: a scintillator for high-rate applications, Nuc. Instr. Meth, 1990, v. A287, 606 - 612.
2.12. Kobayashi M., Carlson P., Berglund S., Temperature dependence of CsI:Tl scintillation yields for cosmic muons, 5 and 1.25 MeV γ-rays, Nucl. Instr. Meth., 1989, v. A281, 192 - 196.
2.13. Valentine J.D., Moses W.W., Derenzo S.E., Wehe D.K., Knoll G.F., Nucl. Instr. Meth., 1993, v. A325, 147.
2.14. Ishibashi H., Shimizu K., Susa K., Kubota S., Cerium doped GSO scintillators and its application to position sensitive detectors , IEEE Trans. Nucl. Sci., 1989, NS-36, No. 1, 170 - 172.
2.15.Melcher C.L., Schweitzer J.S., Utsu T., Akiyama S., Scintillation properties of GSO, IEEE Trans. Nucl. Sci., 1990, NS-37, 161 - 164.
2.16. Gwin R., Murray R.B., Scintillation process in CsI:Tl. I. Comparison with activator saturation model , Phys. Rev., 1963, v. 131, No. 7, 501 -508.
2.17. CLEO Collaboration, CLEO II-Updated proposal, CLN85/634 (1985).
2.18. Schotanus P., Kamermans R., Dorenbos P., Scintillation characteristics of pure and Tl-doped CsI crystals, IEEE Trans. Nucl. Sci., 1990, NS-37(2) 177 - 182.
2.19. Swank R.K., Characteristics of scintillators, Ann. Rev. Nucl. Sci 4 (1954) 111 - 140.
2.20. Visser R., Dorenbos P., van Eijk C.W.E., Hollander R.W., Schotanus P., Scintillation properties of Ce^{3+} doped BaF_2 crystals, IEEE Trans. Nucl. Sci., 1991, NS-38(2) 178 - 183.
2.21. Tailor R.S., Nestor O.H., Utts B., Investigation of cerium-doped barium fluoride, IEEE Trans. Nucl. Sci., 1986, NS-33, No. 1, 243 - 246.
2.22. Zizong X., Zhufang G., Jin C., Caoshu S., Dingzhong S., Xianglong Y., Zhiwen Y., Studies on decay time of fluorescence from a series of Ce-doped BaF_2 crystals, Nucl. Instr. Meth., 1992, v. A322, 239 -242.
2.23. Dorenbos P., van Eijk C.W.E., Hollander R.W., Schotanus, P., Scintillation properties of Nd^{3+} doped LaF_3 crystals, IEEE Trans. Nucl. Sci., 1990, NS-37, No. 2, 119.
2.24. Schotanus P., van Eijk C.W.E., Hollander R.W, Pijpelink J., Temperature dependence of BaF_2 scintillation light yield, Nucl. Instr. Meth., 1985, v. A238, 564 - 565.
2.25. Valbis Ya.A., Rachko Z.A., Yansons Ya.L., Vacuum ultraviolet cathodoluminescence of KF, $KMgF_3$ and $KCaF_3$ crystals (cross-luminescence), Opt. Spectrosc., 1988, v. 64, 714 - 715.
2.26. Woody C.L., Levy P.W., Kierstead J.A., Skwarnicki T., Sobolewski Z., Goldberg M., Horwitz N., Souder P., Anderson D.F., Readout techniques

and radiation damage of undoped cesium iodide, IEEE Trans. Nucl. Sci., 1990, NS-37, 492 - 499.

2.27. Kubota S., Ruan(Gen) J., Itoh M., Hashimoto S., Sakuragi S., A new type of luminescence mechanism in large band-gap insulators:proposal for fast scintillation materials, Nucl. Instr. Meth., 1990, v. A289, 253 - 260.

2.28. Schotanus P., Dorenbos P., van Eijk C.W.E., Hollander R.W., Recent developments in scintillator research, IEEE Trans. Nucl. Sci., 1989, NS-36, 132 - 136.

2.29. Kobayashi M., Ishii M., Krivandina E.A., Litvinov M.M., Peresypkin A.I., Prokoshkin Yu.D., Rykalin V.I., Sobolev B.P., Takamatsu K., Vasil'chenko V.G., Cerium fluoride, a highly radiation-resistive scintillator, Nucl. Instr. Meth., 1991, v. A302, 443 - 446.

2.30. Murakami T., Kasagi J., Tachibanaki H., Yoshida K., Shibata Y., Nakagawa T., Ogihara M., Leek S.M., Kubo T., Motobayashi T., Properties of BaF_2 scintillators in charged particle detection, Nucl. Instr. Meth., 1986, v. A253, 163 - 165.

2.31. Kobayashi H., Konaka A., Miyake K., Nakamura T.T., Sasao N., Yamashita T., Fukushima Y., Nomachi M., Sasaki O.S., Tanguchi T., Test of BaF_2 scintillators coupled to a photomultiplier with a CsTe photocatode, Nucl. Instr. Meth., 1988, v. A270, 106 - 109.

2.32 Woody C.L., Lewy P.W., Kierstead J.A., Slow component suppression and radiation damage in doped BaF_2 crystals, IEEE Trans. Nucl. Sci., 1989, NS-36, 536 - 542.

2.33. Sugimoto S., Fukai K., Mori K., Ide S., Kaneko H., Takaki H., Kobayashi M., Detection of fast pulse from BaF_2 calorimeters, Nucl. Instr. Meth., 1993, v. A336, 179-185.

2.34. Nambissan P.M.G., Sengupta A., Sen P., Parkhurst P.A., Energy/time measurements with BaF_2 and RCA C31024 PMT, Nucl. Instr. Meth., 1989, v. B40/41, 1211 - 1213.

2.35. Dafni E., Nucl. Instr. Meth., 1987, v. A254, 54.

2.36. Lorenz E., Mageras G., Vogel H., Test of a barium fluoride calorimeter readout between 2 and 40 GeV incident energy, Nucl. Instr. Meth., 1986, v. A249, 235 - 240.

2.37. Anderson D.F., Bouclier R., Charpak G., Majewski S., Kneller G., Coupling of a BaF_2 scintillator to a TMAE photocathode and a low-pressure wire chamber, Nucl. Instr. Meth., 1983, v. 217, 217 - 223.

2.38. Bouclier R., Charpak G., Wao G., Million G., Mine P., Paul S., Santiard J.C., Scigocki D., Solomey N., Suffert M., Test of an electromagnetic calorimeter using BaF_2 scintillators and photosensitivewire chambers between 1 and 9 GeV, Nucl. Instr. Meth., 1988, v. A267, 69 - 86.

2.39.Buzulutskov A.F., Turchanovich L.K., Vasil'chenko V.G., Coupling of a BaF_2 scintillator to a wire chamber filled with thriehylamine, Nucl. Instr. Meth., 1989, v. A281, 99 - 102.

2.40. Charpak G., Mine P., Peskov V., Scigocki D., Valbis J., BaF_2 calorimeters with photosensitive gaseous chambers, Proc. ECFA Study Week on Instrumentation Technology for High-Luminosity Hadron Colliders, Barcelona, September 1989, CERN 89-10, 588 - 592.

2.41. Ishibashi H., Mechanism of luminescence from a cerium-doped gadolinium orthosilicate (Gd_2SiO_5) scintillator, Nucl. Instr. Meth., 1990, v. A294, 271 - 277.

2.42. Suzuki H., Tombrello T.A., Melcher C.L., Schweitzer J.S., UV and gamma-ray excited luminescence of cerium-doped rare-earth oxyorthosilicates, Nucl. Instr. Meth., 1992, v. A320, 263 - 272.

2.43. Bolinger L.M., Thomas G.E., Measurement of time dependence of scintillation intensity by a delayed-coincidence method, Rev. Sci. Instr., 1961, v. 32, No. 9, 1044 - 1050.

2.44. Moszynsky M., Bengtson B., Light pulse shapes from plastic scintillators, Nucl. Instr. Meth., 1977, v. 142, 417 - 434.

2.45. Moszynsky M., Vacher J., Odru R., Application of the HR 400 microchannel plate photomultiplier to study the light pulse shape from fast and slow scintillators by means of the single photon method, Nucl. Instr. Meth., 1982, v. 204, **141** - 147.

2.46. Storm E., Israel H.I., Photon cross sections from 1 KeV to 100 MeV for elements Z = 1 to Z = 100, Nucl. Data Tables, 1970, v. A7, 565 - 681.

2.47. Rossi B., High Energy Particles, Prentice-Hall, NJ, 1952.

2.48. Longo E., Sestili I., Monte Carlo calculation of photon-initiated electromagnetic showers in lead glass, Nucl. Instr. Meth., 1975, v. 128, 283 - 307.

2.49. Yuda T., Electron-induced cascade showers in inhomogeneous media, Nucl. Instr. Meth., 1969, v. 73, 301 - 312.

2.50. Kobayashi M., Kondo K., Hirabayashi H., Kurokawa S., Taiono M., Yamamoto A., Sugimoto S., Yoshida H., Wada T., Nakagawa Y, Ogawa M., Ishii M., Akiyama S., Ishibashi H., Radiation damage of BGO crystals due to low energy γ-rays, high energy photons and fast neutrons, Nucl. Instr. Meth., 1983, v. 206, 107 - 117.

2.51. Majewski S., Anderson D., Radiation damage test of barium fluoride scintillator, Nucl. Instr. Meth., 1985, v. A241, 76 - 79.

2.52. Zhu R.Y., On quality requirements to the barium fluoride crystals, CIT report, CALT-68-1767, 1992, p. 45.

2.53. Ma D.A., Zhu R.Y., On optical bleaching of barium fluoride crystals CIT report, CALT-68-1812, 1992, p. 23.

2.54. Kobayashi M. et al., Radiation hardness of cerium-doped gadolinium silicate Gd_2SiO_5:Ce against high energy protons, fast and thermal neutrons, Nucl. Instr. Meth., 1993, v. A330, 115 - 120
2.55. Antipov A.V., Britvich G.I., Chumakov A.A., Vasilchenko V.G., Buchinskaya I.I., Krivandina E.A., Sobolev B.P., Zhmurova Z.I., Devitsin E.G., Kozlov V.A., Krechko Yu.A., Motin Yu.D., Investigation of new inorganic materials for homogeneous electromagnetic calorimeters, Nucl. Instr. Meth., 1993, v. A327, 346 - 353
2.56. Amelinckx S., Radiation effects in ionic crystals, Proc. International School of Phys. "Enrico Fermi", v.18, Academic Press, New York, 1962, p.p. 422 - 427
2.57. Mitchell E.W.J., Radiation damage in covalent crystals, Proc. International School of Phys. "Enrico Fermi", v.18, Academic Press, New York, 1962, p.p. 518 - 545
2.58. Lecoq P., Li P.J., Rostaing B., BGO radiation damage effects: optical absorption, thermoluminescence and thermoconductivity, Nucl. Instr. Meth., 1991, v. A300, 240 - 258
2.59. Pong W., Inouye C.S., Okada S.K., Ultraviolet photoemission studies of BaF_2 and $BaCl_2$, Phys. Rev. B, 1978, v. 18, No. 8, 4422 - 4425
2.60. Murakami A., Asakura H., Yoshinaka Y., Radiation damage and recovery in the light emittance efficiency and the attenuation length of barium fluoride scintillator, Nucl. Instr. Meth., 1991, v. A301, 435 - 444
2.61. Kobayashi M., Ishii, M., Effect of cerium doping on the radiation hardness of gadolinium silicate Gd_2SiO_5:Ce, Nucl. Instr. Meth., 1993, v. B82, 85 - 90
2.62. Wei Z.Y., Zhu R.Y., Newman H., Yin Z.W., Light yield and surface treatment of barium fluoride crystals, Nucl. Instr. Meth., 1991, v. B61, 61 - 66
2.63. Sakuragi S. (Union Material); private communication.